底面亂流境界層의 底質移動特性

On the sediment transport characteristics of
the bottom turbulent boundary layer

金南亨* ・ 瀧川清**
Kim, Nam Hyeong ・ Kiyoshi Takikawa

Abstract

A finite element method(FEM) is presented and applied to the two-dimensional bottom turbulent boundary layer. The time-dependent incompressible motion of a viscous fluid is formulated by using the well-known Navier-Stokes equations and vorticity equation in terms of the velocity and pressure fields. The general numerical formulation is based on Galerkin method and solved by introducing the mixing length theory of Prandtl for eddy kinematic viscosity of a turbulent flow field. Numerical computations of the transport of sediment on an arbitrary sea-bed due to wave motion in the turbulent boundary layer are carried out. The results obtained by the FEM made clear the difference in characteristic features between the boundary layer due to oscillatory flow and the boundary layer due to wave motion.

요 지

본 논문에서는 유한요소법을 2차원 난류경계층에 적용하였으며, 점성유체의 시간의존 비압축성 운동을 시간과 압력장(場)에서 Navier-Stokes방정식과 vorticity방정식을 이용하여 정식화하였다. 수치계산방법은 Galerkin방법에 기초하였으며, 난류 경계층의 eddy kinematic viscosity에 대해서는 Prandtl의 혼합거리이론을 도입하였다. 난류 경계층에서 파동에 의한 임의 저면에서 저질의 이동을 수치계산하였다. 유한 요소법에 의해 얻어진 결과는 진동흐름에 의한 경계층과 파동에 의한 경계층에서의 특성의 차이를 분명히 하였다.

1. Introduction

In order to understand mechanisms of sediment movement as well as energy dissipation, it is essential to elucidate characteristics of the boundary

* 정회원・清州大學校 海洋科學大學 海洋土木工學科, 專任講師
** 日本 熊本大學 工學部 土木環境工學科, 教授
Non-membership, Professor, Ph.D. Dept. of Civil and Environmental Eng., Faculty of Eng., Kumamoto University, Kumamoto 860, JAPAN

layer flow over sand-rippled beds. However, our knowledge on the boundary layer flow over sand-rippled beds is still limited due to the complicated features of the boundary layer flow which involve vortices and turbulence. As a basis of the investigation of this object, effective numerical simulation techniques combined with the progress of large-sized computer are required for the analysis of the complicated boundary layer varying in time

and space. Although finite difference methods still dominate most of this field at present, the applications of finite element method to fluid mechanics for stable and accurate computations seem to be increasing. Recently, numerical research efforts have been made by many researchers to formulate and apply the boundary layer flow analysis(see e.g. References 1-6). Much of those work has been related to the solution of the so-called(k, ε) turbulence model in conjunction with the Reynolds averaged momentum equations. In addition, many of these finite element analyses have concentrated on the solution of the steady-state form of these equations.

It seems that there are no analytical examples for a boundary layer over sand-ripples with boundary conditions due to wave motion, but there is a difference between oscillatory flow and wave motion in the boundary layer. The objective of the present study is to describe the characteristics in this boundary layer. The turbulent boundary layer on sea-beds of arbitrary shape for arbitrary mean flow is analyzed using the finite element method based on Galerkin method. Several numerical computations are carried out. The results of oscillatory flow and those of wave motion for boundary layer on a sea-bed are compared.

2. Numerical analysis

2.1 Formulation by FEM

We consider the turbulent boundary layer flow on an arbitrary sea-bed in a two dimensional domain with the coordinates taken such that the x-axis coincides with the horizontal oriented positively to the right and the y-axis coincides with the vertical oriented positively upwards, and the origin is at the bottom. In the case of two-dimensional, incompressible and turbulent flow by introducing into the Navier-Stokes equations(N-S equation) for the mean flow, we obtain the following system of differential equations :

$$\frac{\partial u}{\partial t} + u \frac{\partial u}{\partial x} + v \frac{\partial u}{\partial y} = F_x - \frac{1}{\rho} \frac{\partial p}{\partial x} + \frac{\partial}{\partial x}$$

$$\{(v+\varepsilon_\tau) \frac{\partial u}{\partial x}\} + \frac{\partial}{\partial y} \{(v+\varepsilon_\tau) \frac{\partial u}{\partial y}\} \qquad (1)$$

$$\frac{\partial v}{\partial t} + u \frac{\partial v}{\partial x} + v \frac{\partial v}{\partial y} = F_y - \frac{1}{\rho} \frac{\partial p}{\partial y} + \frac{\partial}{\partial x}$$

$$\{(v+\varepsilon_\tau) \frac{\partial v}{\partial x}\} + \frac{\partial}{\partial y} \{(v+\varepsilon_\tau) \frac{\partial v}{\partial y}\} \qquad (2)$$

where velocity u and v denote the mean velocity in x-direction and y-direction, respectively, and are unknown variables in the above equation. ρ is the density, p is the pressure, v is the kinematic viscosity, ε_τ is the eddy kinematic viscosity, and F_x and F_y are the mass force. There is a lot of controversy concerning the estimation of this ε_τ. A number of models with respect to ε_τ have been proposed. As a simplified model, we treat Reynolds stress in the turbulence as Prandtl's mixing length theory[7] in this paper. The estimation of ε_τ can be expressed as

$$\varepsilon_\tau = l^2 \left| \frac{\partial u}{\partial y} \right| \qquad (3)$$

To make use of this equation it is necessary to adopt some expression for the mixing length l. The scale of the turbulent eddies increases with the distance from the bottom boundary. The most obvious assumption is

$$l = ky \qquad (4)$$

where the constant k is the Karman constant, which we take equal to 0.4 y , and is the distance from the bottom boundary along the x-direction. For analytical stability and easy treatment, the vorticity equation in present paper is induced and used. By differentiating the eq.(1) with respect to y and eq.(2) with respect to x, the pressure term and the mass force term are eliminated from the N-S equations and the vorticity equation is obtained as

$$\frac{\partial w}{\partial t} + u \frac{\partial w}{\partial x} + v \frac{\partial w}{\partial y} =$$

$$\frac{\partial}{\partial x} \{(v+\varepsilon_\tau) \frac{\partial w}{\partial x}\} + \frac{\partial}{\partial y} \{(v+\varepsilon_\tau) \frac{\partial w}{\partial y}\} \qquad (5)$$

where

$$w = \frac{\partial v}{\partial x} - \frac{\partial u}{\partial y} \qquad (6)$$

w is the vorticity and is positive counter-clockwise. From the above assumptions, the continuity equation is given as

$$\frac{\partial u}{\partial x} + \frac{\partial v}{\partial y} = 0 \qquad (7)$$

The relationship between the velocity component u and v and the stream function ψ can be described as :

$$u = \frac{\partial \psi}{\partial y}; \quad v = -\frac{\partial \psi}{\partial x} \qquad (8)$$

Substituting eq.(8) into eq.(6), the new equation with respect to vorticity w and stream function ψ is obtained as follows :

$$\nabla^2 \psi = -w \qquad (9)$$

where ∇^2 represents the following differential operator.

$$\nabla^2 = \frac{\partial^2}{\partial x^2} + \frac{\partial^2}{\partial y^2}$$

In order to eliminate velocity u and v from eq. (5), we substitute and eq.(8) into eq.(5). Accordingly, the turbulent vorticity equation of the unknown quantity related to stream function ψ and vortex w is given as follows :

$$\frac{\partial w}{\partial t} + (\frac{\partial \psi}{\partial y}\frac{\partial w}{\partial x}) - (\frac{\partial \psi}{\partial x}\frac{\partial w}{\partial y}) = (v+\varepsilon_\tau)\nabla^2 w \ (10)$$

Using the weighted residual method, eqs.(9) and (10) are written in the following manner :

$$\int_\Omega \psi_* \nabla^2\psi d\Omega + \int_\Omega \psi_* w d\Omega = 0 \qquad (11)$$

$$\int_v w_* \frac{\partial w}{\partial t}d\Omega + \int_\Omega w_*(\frac{\partial \psi}{\partial y}\frac{\partial w}{\partial x} - \frac{\partial \psi}{\partial x}\frac{\partial w}{\partial y})$$
$$- \int_\Omega w_*(v+\varepsilon_\tau)\nabla^2 w d\Omega = 0 \qquad (12)$$

where ψ_* and w_* are the weighting functions. By partial integrations using the Green-Gauss theorem, we have correspondingly

$$\int_\Omega \nabla\psi_*\nabla\psi d\Omega - \int_\Omega \psi_* w d\Omega - \int_\Gamma \psi_* \frac{\partial \psi}{\partial n}d\Gamma = 0 \ (13)$$

$$\int_\Omega w_* \frac{\partial w}{\partial t}d\Omega + \int_\Omega w_*(\frac{\partial \psi}{\partial y}\frac{\partial w}{\partial x} - \frac{\partial \psi}{\partial x}\frac{\partial w}{\partial y})d\Omega$$
$$+ \int_\Omega (v+\varepsilon_\tau)\nabla w_*.\nabla w d\Omega - \int_\Gamma (v+\varepsilon_\tau)w_* \frac{\partial w}{\partial n}d\Gamma = 0 (14)$$

The domain of analysis is divided into triangular elements. The unknown quantities ψ, ψ_*, w and w_* employing linear function are approximated inside the triangle element such that

$$\psi = \sum_{i=1}^3 \phi_i\psi_i = \phi^T\psi, \quad \psi_* = \sum_{i=1}^3 \phi_i\psi_{*i} = \phi^T\psi_*$$
$$w = \sum_{i=1}^3 \phi_i w_i = \phi^T w, \quad w_* = \sum_{i=1}^3 \phi_i w_{*i} = \phi^T w_*$$

in which ϕ_i is the interpolation function. ψ_i, ψ_{*i}, w_i and w_{*i} are the nodal values. The shape of the interpolation function is

$$\phi_\alpha = \frac{1}{2\Delta^e}(a_\alpha + b_\alpha x + c_\alpha y) \ (\alpha = 1,2,3) \qquad (16)$$

in which Δ^e is the area of triangle element, and a_α, b_α and c_α are the coefficients decided in each element. Substituting eq.(15) into eqs.(13) and(14), the element equations are obtained as

$$\sum_{\beta=1}^3 D_{\alpha\beta}\psi_\beta - \sum_{\beta=1}^3 M_{\alpha\beta}w_\beta - \Gamma_{2\alpha} = 0 \qquad (17)$$

$$\sum_{\beta=1}^3 M_{\alpha\beta}\dot{w}_\beta + \sum_{\beta=1}^3 A_{\alpha\beta}w_\beta + \sum_{\beta=1}^3 (v+\varepsilon_\tau)D_{\alpha\beta}w_\beta - \Gamma_{4\alpha} = 0$$
$$(\alpha = 1,2,3)$$

where

$$\dot{w}_\beta = \frac{dw_\beta}{dt},$$

$$\left. \begin{array}{l} A_{\alpha\beta} = \int_e \phi_\alpha(\sum_{r=1}^3 \frac{\partial \phi_r}{\partial y}\psi_r \frac{\partial \phi_\beta}{\partial x} - \sum_{r=1}^3 \frac{\partial \phi_r}{\partial x}\psi_r \frac{\partial \phi_\beta}{\partial y})d\Omega \\[2mm] M^{\alpha\beta} = \int_e \phi_\alpha\phi_\beta d\Omega, \\[2mm] D_{\alpha\beta} = \int_e (\frac{\partial \phi_\alpha}{\partial x}\frac{\partial \phi_\beta}{\partial x} + \frac{\partial \psi_\alpha}{\partial y}\frac{\partial \psi_\beta}{\partial y})d\Omega \\[2mm] \Gamma_{2\alpha} = \int_\Gamma \phi_\alpha \frac{\partial \psi}{\partial n}d\Gamma, \\[2mm] \Gamma_{4\alpha} = \int_\Gamma (v+\varepsilon_\tau)\phi_\alpha \frac{\partial w}{\partial n}d\Gamma \end{array} \right\} (19)$$

After discretization eqs.(17) and(18) for the all elements by a conventional procedure, the system equations can be written in the following matrix form :

$$[A]\psi - [M]w - \Gamma_2 = 0 \qquad (20)$$

$$[M]\dot{w} + [A]w + (v + \varepsilon_\tau)[D]w - \Gamma_4 = 0 \qquad (21)$$

where matrix $[D]$, $[M]$ and $[A]$ are the total matrix with respect to the element $D_{\alpha\beta}$, $M_{\alpha\beta}$ and $A_{\alpha\beta}$ respectively. Γ_2 and Γ_4 are the natural boundary conditions.

After some manipulation, the matrix becomes of the banded type here. Therefore, the simultaneous equations obtained from eqs.(20) and(21) must be sloved. In order to solve the simultaneous equations, we employ the incremental method which is used widely in the analysis of non-linear field problems since the matrix $[A]$ in eq.(21) includes a non-linear term of unknown ψ. Here we defined the increments $\Delta\psi$ and Δw between two successive time instant t_0 and $t_0 + \Delta t$, as follows

$$\psi = \psi_0 + \Delta\psi$$
$$w = w_0 + \Delta w \qquad (22)$$

where ψ_0, w_0 and ψ, w are the values of ψ, w at the time t_0 and $t_0 + \Delta t$, respectively. Also, a finite difference form for the time term in eq.(21) can be taken as

$$\dot{w} = \frac{2(w - w_0)}{\Delta t} - \dot{w}_0 \qquad (23)$$

in which the subscript 0 denotes a value at the time $t - \Delta t$. For simplicity, Δt is fixed. In order to leave the characteristics of implicit scheme, first, if we impose the n-th approximate value of w, we can seek the n+1st approximate value of ψ in eq.(20). Secondly, if we give the n-th approximate value of ψ, we can find the n+1st approximate value of w in eq.(21). By doing so, we can use the semi-implicit scheme iterating until the convergence criterion is satisfied. The following convergence criterion at each time step is given

$$\text{MAX}_j \left| \frac{w_j^{n+1} - w_j^n}{w_j^n} \right| < \in, \quad j = 1, 2, \cdots, N_t \quad (24)$$

where N_t is the total number of nodal points and the superscript n indicates the n-th iteration. In the present examples, the parameter $\in$ is fixed at 0.01. By this procedure, the computational time is reduced and stable solutions are obtained.

2.2 Boundary conditions

Boundary conditions must be given as either essential boundary conditions or natural boundary conditions for ψ and w on the boundary in the analytical domain. A rectangular shape domain as shown Fig. 1 is selected with a height and length 15 cm and 48 cm respectively. Here in order to obtain the exact results, we divide the parts from bottom boundary to height into finer mesh, exactly 2 times, than other parts. The region is divided into triangles whose spacings are set to be uniform in x-axis and to be different in y-axis owing to the location of the nodal point over sand-ripple. The boundary of analytical domain is defined as follow; A-B as the input boundary, B-C as the bottom boundary, C-D as the output boundary, and A-D as the free surface boundary. We assume the boundary conditions were taken from the theory of the linear laminar flow. That is why it is impossile to establish the boundary conditions of the turbulent flow till now. In order to eliminate the influence by introducing the boundary conditions of the linear laminar flow, we take the wider domain than virtual domain needed in analysis. From the theory of the laminar flow, the N-S equation, the continuty equation and the equation of motion at the outer edge of the boundary layer is expressed below.
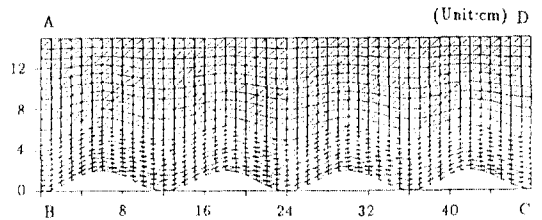

Fig. 1. Finite element mesh for computation region.

$$\frac{\partial u}{\partial t} + u\frac{\partial u}{\partial x} + v\frac{\partial u}{\partial y} = -\frac{1}{\rho}\frac{\partial p}{\partial x} + \frac{1}{\rho}\frac{\partial \tau}{\partial y} \quad (25)$$

$$\frac{\partial u}{\partial x} + \frac{\partial v}{\partial y} = 0 \quad (26)$$

$$\frac{\partial u_b}{\partial t} + u_b\frac{\partial u_b}{\partial x} = -\frac{1}{\rho}\frac{\partial p}{\partial x} \quad (27)$$

where u_b is the velocity at the outer edge of the boundary layer. in eq.(25) and in eq.(27) are smaller than other terms, therefore they are neglected. For laminar flow, the shear stress is defined as

$$\frac{\tau}{\rho} = v\frac{\partial u}{\partial y} \quad (28)$$

Combining eqs.(25) and(27), we have

$$\frac{\partial u}{\partial t} = -\frac{\partial u_b}{\partial t} + v\frac{\partial^2 u}{\partial y^2} \quad (29)$$

The velocity distribution at the bottom boundary taking $y = -h$ by the theory of the small amplitude wave is

$$u_b = \frac{\sigma H}{2\sinh kh}\cos(kx - \sigma t) \quad (30)$$

With the above equation, the solution to eq.(29) is

$$u = \frac{\sigma H}{2\sinh kh}\{\cos(kx\text{-}\sigma t) - \exp^{-\beta y}\cos(kx - \sigma t + \beta y)\} \quad (31)$$

where $\beta = \sqrt{\dfrac{\sigma}{2v}}$, and $\sigma = \dfrac{2\phi}{T}$. k is the wave number, is the wave height, and h is the water depth. The stream function ψ_L is obtained by integrating the eq.(31)

$$\psi_L = \int_0^y u(y)dy$$

$$= \frac{\sigma H}{2\sinh kh}\int_0^y \{\cos(kx - \sigma t) - \exp^{-\beta y}\cos(kx - \sigma t + \beta y)\}dy$$

$$= \frac{\sigma H}{2\sinh kh}\Big[\cos(kx - \sigma t)y + \frac{\exp^{-\beta y}}{2\beta}\{\cos(kx - \sigma t + \beta y) - \sin(kx - \sigma t + \beta y)\}$$

$$- \frac{1}{2\beta}\{\cos(kx - \sigma t) - \sin(kx - \sigma t)\}\Big] \quad (32)$$

While the vorticity w_L is obtained by differentiation eq.(31) with repect to y

$$w_L = -\frac{du(y)}{dy}$$

$$= -\frac{\partial}{\partial y}\Big[\frac{\sigma h}{2\sinh kh}\{\cos(kx - \sigma t) - \exp^{-\beta y}\cos(kx$$

$$-\sigma t + \beta y)\}\Big]$$

$$= \sqrt{2}\frac{\beta\sigma H}{2\sinh kh}\{\exp^{-\beta y}\cos(kx - \sigma t + \beta y - \frac{\pi}{4})\} \quad (33)$$

Table 1. Details of the boundary conditions

Boundary condition	Side	Upper	Bottom
Stream function ψ	ψ_L	ψ_L	0
Vortivity w	w_L	w_L	w_B

Using the Taylor expansion of ψ for the bottom boundary B-C, Briley equation is introduced as

$$w_B = \frac{-85\psi_B + 108\psi_1 - 274\psi_2 + 4\psi_3}{18\Delta y^2} \quad (34)$$

where ψ_B is the value at the bottom boundary, and and is the value of nodal point corresponding to increment Δy. With the eqs.(32), (33) and(34) the boundary conditions are taken as shown in Table 1. Where ψ_L and w_L are the values computed by the theory of the linear laminar flow except that ψ_L isn't alloted on the upper boundary in the case of oscillatory flow. There exists vorticity w_B on the bottom for the sake of non-slip conditions.

3. Numerical results and discussions

3.1 Computational examples

In the analysis of the sea-bed model, sinusoidal sand-ripples and unsymmetrical sand-ripples have been considered as shown in Fig.2. Computations were carried out for the cases of the oscillatory flow employing a sinusoidal wave with mean flow, and the wave motion based on the small amplitude wave theory as shown in Table 2. As mentioned previously, because the boundary conditions

Table 2. Details of the numerical computations.

Case No.	Sand-rippled bed	Mean flow condition	Period sed	Depth cm	Height cm	Velocity amplitude cm/sec
1	symmetry	wave motion	1.4	25	8.5	---
2	symmetry	oscillatory flow	1.4	---	---	20.7
3	unsymmetry	wave motion	1.4	25	8.0	---
4	unsymmetry	oscillatory flow	1.4	---	---	20.7

(a) sinusoidal sand-rippled bed

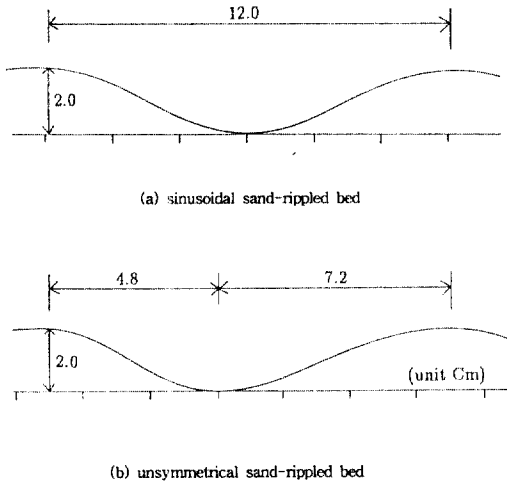(b) unsymmetrical sand-rippled bed

Fig. 2. The profiles of sand-rippled beds.

of the laminar flow is introduced, actually the object of investigation in the analytical domain is limited to the horizontal 32 elements each of 1 cm length and vertical 17 elements; 10 elements each of 0.5 cm and of 7 elements each of 1 cm length. The incremental time interval is taken to be $\frac{1}{200}$ sec per period. We assume that the velocity is considered positive in the direction of the positive x-axis and that the wave is propagating from left to right.

As initial conditions, we assume that the values obtained by the theory of linear laminar flow are used for all nodal points. Fig.3 illustrates the comparison of the phase change of mean velocity field between the calculations and the experiments measured by Hamamoto et al.[8] for a sinusoidal

(a) experimental values [8]
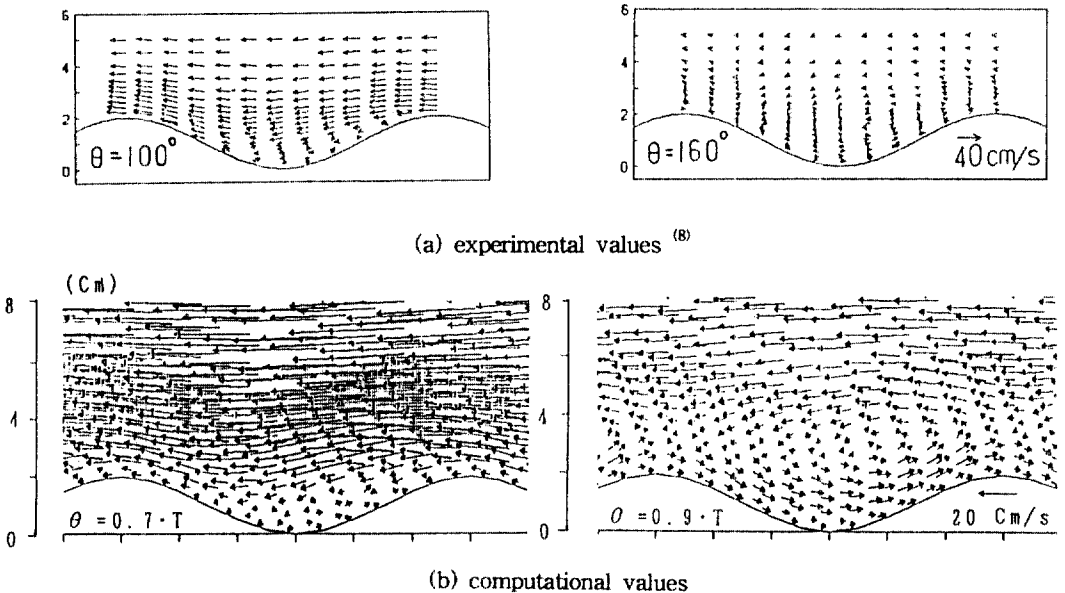

(b) computational values

Fig. 3. Phase change of mean velocity field.

oscillatory flow on the symmetrical sand-ripples. These computation conditions are the same as those of experiments by Hamamoto et al.[8] The mean velocity at the initial phase is decided to be zero at a turning point of time moving from negative zone to positive zone. It seems that the shape of mean velocity vector is well reproduced although its vector differs in size.

3.2 Numerical results

Fig. 4 shows the change of velocity vector varying in time and space during one period, which is computed for the cases of the wave motion and the oscillatory flow with mean flow for the unsymmetrical sand-ripples. Moreover Fig. 4 (a) shows the fluctuation of the surface wave profiles by closed circles and the still water level by dashed lines at each phase. For the case of oscillatory flow as shown in Fig. 4 (b), a clockwise rotational vorticity start to develop at the steep slope of the closest phase from the phase (0.2T) where the mean flow velocity becomes just before the maximum, and vorticity shows the tendency of growth with the decrease of velocity and is inclined to move slightly upwards (0.2T~0.4T). This dissipation of the vortex disappeare when reaching the phase where the velocity direction is reversed. When the velocity increase in the reverse direction, the vortex is formed in an anticlockwise rotational motion in the vicinity of the central part of gentle slope (0.7T). As the velocity decreases, the vortex undergoes the process of growth and disappearence. Meanwhile, for the case of wave motion as shown in Fig. 4(a), if attention is given to the trough part of central sand-ripples, the phases display almost the same change as in the oscillatory flow. However, the vortex develops at the phase where the velocity moving towards the onshore starts decreasing after the wave crest is passed, collides with the vertical velocity and assimilates the velocity moving towards the offshore in which the vortex is not dissipated enough upwards(0.3T~0.5T). Also the vortex formed anticlockwise at the gentle slope is grown in proportion to the decrease in the velocity moving in the offshore direction, is further dissipated upwards with

the vertical stream lines of the mean flow and is absorbed the stream line moving towards the offshore direction in the upper zone (0.8T~0.1T). Therefore the governing factor that may be defined the transport of the suspended sand rolling up by vortex at the sea-bed can be well understood from the vortex process in the wave motion.

Fig. 5 shows the distribution of horizontal velocity on a vertical section on the unsymmetrical sand-ripples. On the section near the central part of gentle slope, the horizontal velocity goes to the maximum value when the velocity changes direction from right to left. The velocity gradient near the sea-bed becomes maximum at the point where the velocity changes direction from left to right and at that time the biggest shear stress would be acting at that point. The mean flow condition hasn't shown a big difference in the horizontal velocity between the oscillatory flow and the wave motion as shown in Fig.5.

Fig.6 shows the loci of water particles during one cycle of motion on the trough section of unsymmetrical sand-ripples using Lagrangian description as denoted by open circles. Since the initial phase of pursuit differ, there is no comparison between case 3 (wave motion) and case 4 (oscillatory flow) in the same mean flow condition. However, for the case of wave motion as shown in Fig. 6 (a), water particles move in the potential elliptical motion. After one cycle of motion the loci is transported towards the onshore. Water particles are moved towards the offshore by the clockwise rotational vortex formed at the coastal slope of sea-bed and are transported towards the onshore with vortex dissipated upwards direction when the phase is reversed. On the other side, for the case of oscillatory flow as shown in Fig.6 (b), water particles in the upper layers move horizontally back and forth. At the lower layers the water particles move into the gentle slope by the velocity oriented to the left. Some water particles are transported to the right on a large scale by the anticlockwise rotational vortex, because this vortex disappear when the mean flow is reversed other water particles are, on the average, transported into the gentle slope, where they can not
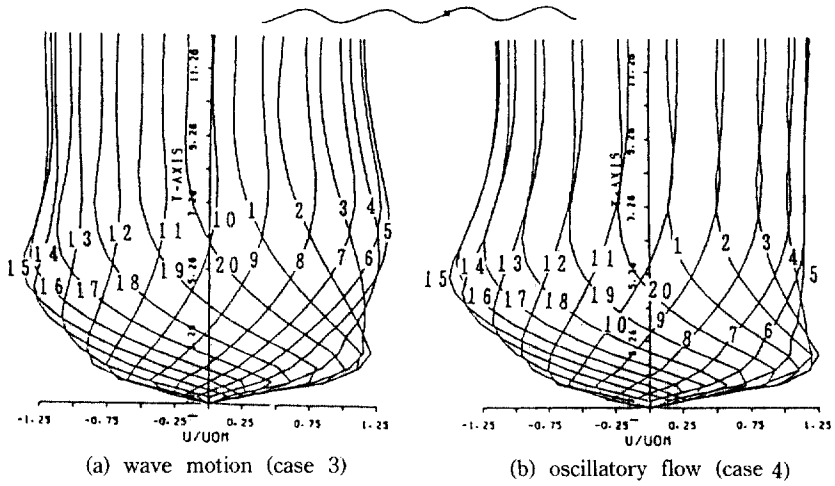
offshore   onshore
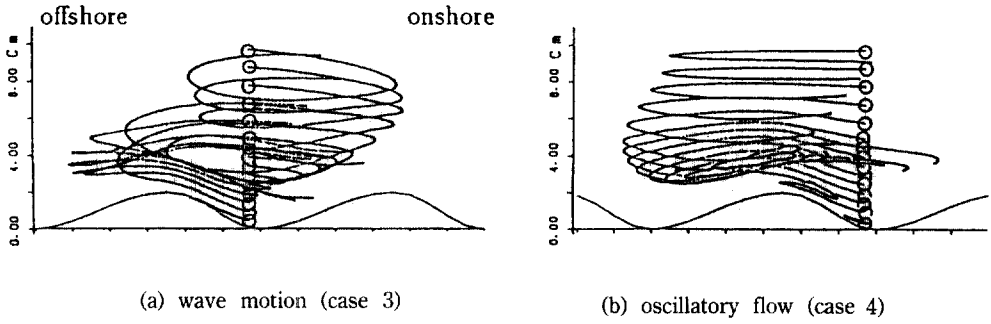
(a) wave motion(case 3)   (b) oscillatory flow(case 4)

Fig. 4. Time history of men velocity displacements.

(a) wave motion (case 3)　　　　(b) oscillatory flow (case 4)

Fig. 5. The horizontal velocity distributions.

(a) wave motion (case 3)　　　　(b) oscillatory flow (case 4)

Fig. 6. The locus of water particles.

(a) numerical computation by Sato et al[9]

(b) wave motion (case 3)　　　　(c) oscillatory flow (case 4)

Fig. 7. The transport of water particles.

offshore onshore

(a) wave motion (case 1)

(b) oscillatory flow (case 2)

(c) wave motion (case 3)

(d) oscillatory flow (case 4)
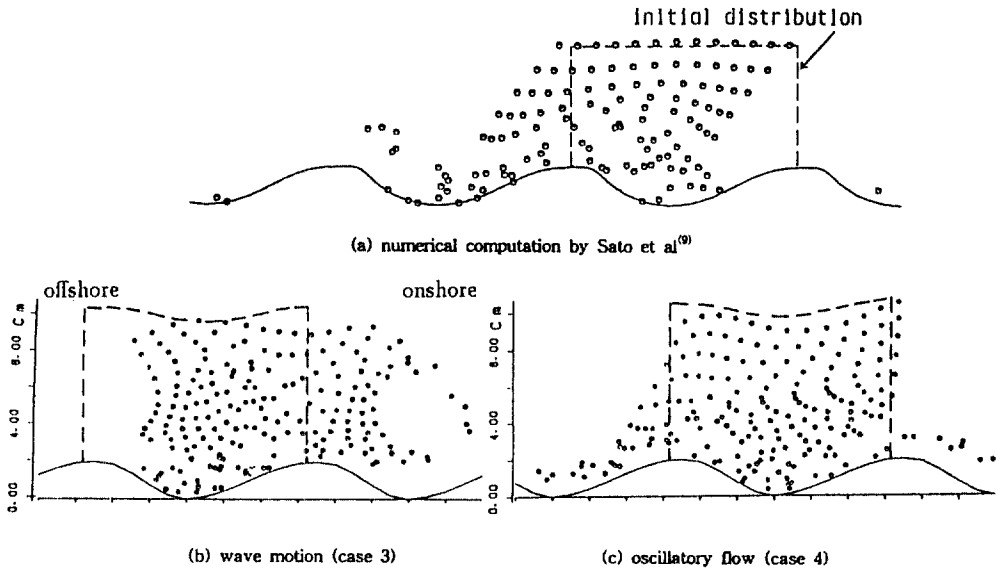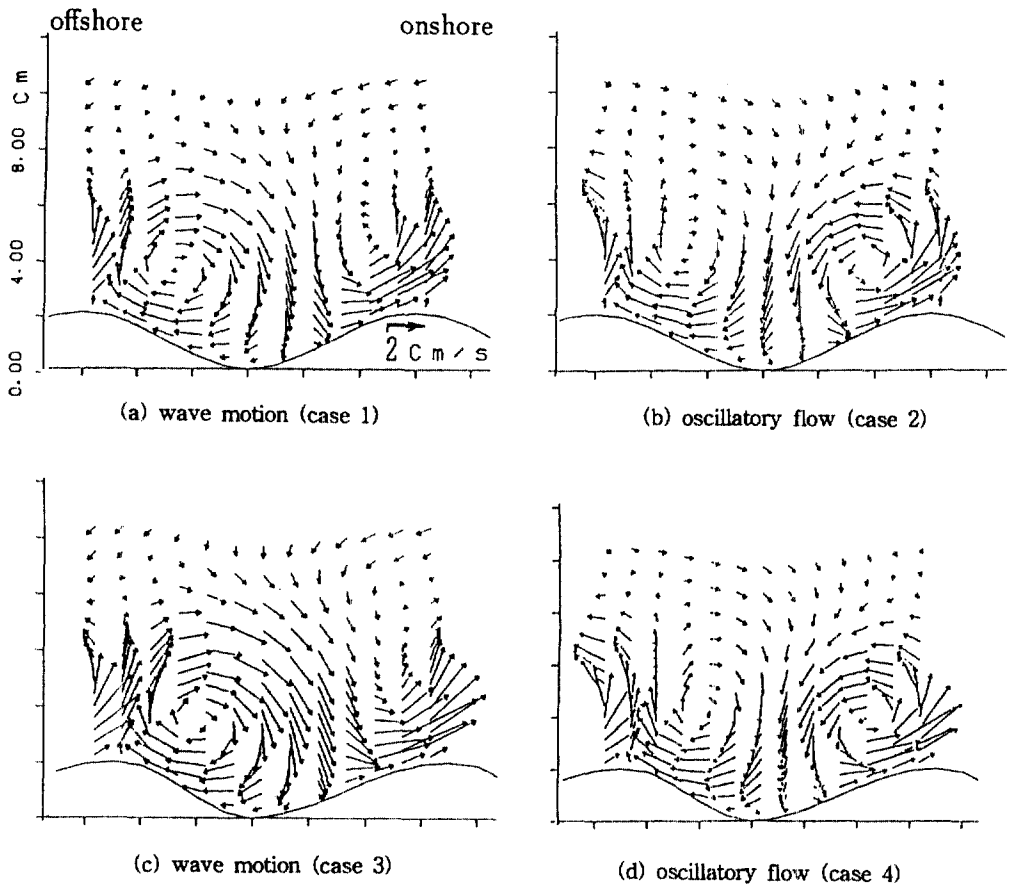
Fig. 8. The velocity fields of steady flow.

return back to the initial phase.

Fig.7 shows the calculated positions of water particles after one period which start at $\theta=0$ from nodal points in the analytical domain encircled by broken lines. The transport of each water particle is calculated with Lagrangian description as mentioned in Fig.6. For the case of mean flow due to wave motion, water particles are transported to the onshore, while for the case of mean flow due to oscillatory flow, the water particles in the sea-beds are transported into gentle slope, which shows the same tendency with the result obtained by Sato et al.[9] using the finite difference method. This tendency of the transport of water particles, for instance similar results are obtained in case 1 and 2 for symmetrical sand-ripples, represents one of the characteristic features by disa-

greement in the mean flow conditions. It is necessary to investigate various cases since the transport of water particles depends on the mean flow amplitude, the mean flow wave profiles, the sand-ripples length and the mean flow velocity etc.

Fig. 8 shows the velocity fields of steady flow obtained from the mean velocity during one period at each point. For oscillatory flow, a couple of vorticity is seen nearly symmetrical without regard to the sand-ripples shape. On the other hand, for wave motion, the steady vorticity exists at the coastal slope and the strong current is seen to run-up the ocean slope. In the results obtained by the numerical computation, it seems that the present solution agrees qualitatively well with the former research and shows the real discharge-duration profiles in the flow fields.

4. Conclusions

Numerical model was presented to calculate the turbulent boundary layer flow as well as laminar boundary layer flow over rippled beds by using the mixing length theory. The validity of the model was confirmed by comparing the mean velocity field and the transport of water particles. Also, these results obviously display the flow pattern at the interior boundary layer with arbitrary mean flow conditions on the arbitrary sea-beds and clearly show the difference of some characteristics between the oscillatory flow layer and the wave motion layer, which haven't been treated in the former research. The examples given herein turn out that the turbulent flow in boundary layer plays important role in the formation and the transport of suspended sand clouds. However, further works are expected on the improvement of the description of the boundary conditions and on the quantitative analysis of the transport of the suspended sediment. All computations have been carried out on a FACOM M-780 computer at Kyushu University, Japan.

References

1. Soliman, M. J. and Baker, A. J., "Accuracy and convergence of a finite element algorithm for turbulent boundary layer flow", *Comput. Methods. Appl. Mech. Eng.*, 28, pp. 81-102, 1981.
2. Smith, R.M., "On the finite-element calculation of turbulent flow using the k-ε model", *Int. Jour. Numer. Methods Fluids*, 4, pp. 303-319, 1984.
3. Smith, R.M., "A practical method of two-equation turbulence modelling using finite elements", *Int. Jour. Numer. Methods Fluids*, 4, pp. 321-336, 1984.
4. Autret, A., Grandotto, M. and Dekeyser, I., "Finite element computation of a turbulent flow over a two-dimensional backward-facing step", *Int. Jour. Numer. Methods Fluids*, 7, pp. 89-102, 1987.
5 Rodi, W., "*Turbulence models and their application in hydraulics*", IAHR State-of-the-Art Paper, Delft, 1980.
6. Utense, T., "Two-equation(k, ε) turbulence computations", *Int. Jour. Numer. Methods Fluids*, 8, pp. 965-975, 1988.
7. Schlichting, H., "*Boundary layer theory 7th ed.*", McGraw-Hill, New York, pp. 579-583, 1989.
8. Hamamoto, K., Mimura, S. and Watanabe, A., "Laboratory study of oscillatory boundary layer flow above rippled bed(2)", *Proc. 29th Japanese Conf. on the Coastal Eng.*, pp. 254-258, 1982, (in Japanese).
9. Sato, S., Uehara, K. and Watanabe, A., "Numerical simulation of the oscillatory boundary layer flow over ripples by a k-ε turbulence model", *Coastal Eng.* in Japan, Vol. 29, pp. 65-78, 1986.